The structure of the human mitochondrial ribosome

Alexey Amunts[#], **Alan Brown**[#], **Jaan Toots**, **Sjors H. W. Scheres**, and **V. Ramakrishnan**[†]
MRC Laboratory of Molecular Biology, Francis Crick Avenue, Cambridge CB2 0QH, United Kingdom

[#] These authors contributed equally to this work.

Abstract

The highly divergent ribosomes of human mitochondria (mitoribosomes) synthesize 13 essential proteins of oxidative phosphorylation complexes. We have determined the structure of the intact mitoribosome to 3.5 angstrom resolution by single-particle electron cryo-microscopy. It reveals 80 extensively interconnected proteins, 36 of which are specific to mitochondria, and three rRNA molecules. The head domain of the small subunit, particularly the mRNA channel, is highly remodeled. Many intersubunit bridges are unique to the mitoribosome, which adopts conformations involving ratcheting or rolling of the small subunit that are distinct from those seen in bacteria or eukaryotes. An intrinsic GTPase mediates a contact between the head and central protuberance. The structure provides a reference for analysis of mutations that cause severe pathologies, and for future drug design.

Introduction

Mitoribosomes have substantially diverged from bacterial ribosomes, with which they share a common ancestor. They have a reversal in their protein to RNA ratio, as a result of a contraction of ribosomal RNA (rRNA) and acquisition of many additional proteins, which facilitate specific requirements of protein synthesis in mitochondria, such as synthesis of hydrophobic proteins and their co-translational delivery to the membrane (1-3). The atomic structure of the mitoribosomal large subunit (mt-LSU) is known (1-3). However, obtaining a similar high-resolution structure of the entire mitoribosome has been hindered by the conformational variability of the small subunit (mt-SSU). The mt-SSU binds mRNA, is involved in accurate initiation and decoding, and undergoes large-scale conformational changes during the elongation cycle (4). Here we report the structure of the intact human mitoribosome at 3.5 Å resolution by electron cryo-microscopy (cryo-EM) revealing an atomic model for the mt-SSU, the unusual dynamics of the mitoribosome and the molecular details of mitochondria-specific bridges between the two subunits.

Structure determination

To overcome the conformational flexibility of the mt-SSU, we collected 7,528 micrographs from a total of four datasets, including the dataset used to solve the structure of the human

[†]To whom correspondence should be addressed: ramak@mrc-lmb.cam.ac.uk.

mt-LSU (2). Each dataset was initially processed independently with 2D and 3D classification used to remove particles that aligned poorly or corresponded to 'free' mt-LSU. The resultant 884,122 particles were classified further revealing three distinct subpopulations, each resolved to better than 5 Å resolution, in which the mt-SSU adopts different orientational states (Fig. S1).

To improve the quality of the maps further to permit accurate model building we applied masks during refinement. Rather than use all particles, we combined the datasets that extended to 4.0 Å or better with additional views of the mitoribosome extracted from the remaining datasets giving a total of 449,823 particles (Fig. S2A). As the mitoribosome displays preferential orientation on the EM grid including a wider variety of views improved the angular sampling of the reconstructions (Fig. S2B) and resulted in a higher overall resolution than obtained by using all data. Refinement with masks applied over the mt-LSU, mt-SSU and the head domain improved the resolution to 3.3, 3.5 and 3.9 Å, respectively (Fig. 1 and Figs. S2-S3). Although local resolution varies within the maps, even at the periphery the density is sufficient for *de novo* model building (Fig. 1).

Overall structure

The model of the human mitoribosome contains three rRNA molecules (16S mt-LSU rRNA, 12S mt-SSU rRNA and mt-tRNA^{Val}) and 80 proteins, of which 36 are specific to mitochondria. Additionally, most proteins with homologs in bacteria have substantial extensions. The increased protein mass results in a ribosome with a distinct morphology (Fig. 2A), a more extensive protein-protein network of over 200 contacts (Fig. S5) and an rRNA core better shielded from reactive oxygen species.

For the mt-SSU, we are able to locate all reported constituent proteins (30, with 14 specific to mitochondria) with the exception of MRPS36, confirming the recent observation that it is not a mitoribosomal protein (5) (Table S2). Additionally, mS30 is shown to be present as a single copy in the mt-LSU and renamed to mL65 (3) and two further homologs of bS18 to that observed in the mt-LSU are identified (Fig. S6). For the mt-LSU we located two additional proteins, bL31m and mL54, which were previously identified in the porcine mt-LSU (3) and further improved the model at the central protuberance and subunit interface (6).

The mt-SSU lacks homologs of uS4, uS8, uS13, uS19 and bS20. With the exception of uS4, these proteins have not been substituted by mitochondria-specific elements (Fig. 2B). In bacteria, uS13 and uS19 from the head form bridges with the central protuberance and interact with the anticodon stem loop of tRNAs in the pretranslocation state (7). Alternative bridges have been formed by mitochondria specific elements, whereas contacts with tRNA are lost. The mt-SSU is elongated as a result of mitochondria-specific proteins at both extremities (mS29 at the head, and mS27 at the bottom). mS26 forms a distinctive 170 Å long helix that wraps around the body.

The mt-rRNA is about half the size of the bacterial one (Fig. S7). As observed for the mt-LSU, deletion of mt-SSU rRNA segments occurs at sites that can be bridged by short (2-3 nucleotide) sections of rRNA (2) (Fig. S8). The remaining rRNA adopts conformations

consistent with those in bacteria, except for h44 (Fig. 5). This helix is a universal element of ribosomes that forms several inter-subunit bridges as well as part of the decoding center. In bacteria, the lower part of the helix is rigid and anchored by bS20, whereas the middle part forms major intersubunit bridges (B2a, B3, B5 and B6a), and the upper part is flexible being involved in tRNA translocation (8).

In the human mitoribosome, the conformation, coordination and flexibility of the lower part of h44 have diverged extensively (Fig. 5B). In part, this may be a response to the loss of constraints of maintaining a bridge (B6) with mt-LSU rRNA H62, which is absent. The decreased rigidity (as observed through high B-factors) is due to loss of stabilizing interactions including with bS20 and base pair rearrangements. In contrast, the movement of the upper part of h44 is likely restricted by the presence of mS38 (Fig. 5B).

Conformational heterogeneity

Ribosomes are highly dynamic, with a ratchet-like rotation of the SSU correlated with mRNA-tRNA translocation. We compared the three distinct subpopulations in our sample to the classical, non-rotated bacterial ribosome (9) and with each other (Table S3). The majority of human mitoribosomes (class 1, 60%) adopt an orientation that is different from the non-rotated state in bacteria. The small subunits are related by a 7.4° rotation around an axis that runs through h44 and h3 (Fig. S9A). Class 2 (22%) closely resembles the fully ratcheted state observed for the bacterial ribosome (10) (Fig. 3A). It is related to Class 1 by a 9.2° counterclockwise rotation (as viewed from the solvent face of the mt-SSU) with bridge B3 acting as a pivot, as seen in bacteria (11). Class 3 (12%) is related to class 1 by a rotation of 9.5° around the long axis of the mt-SSU (Fig. 3B). This conformational mode is observed in eukaryotic, but not bacterial, ribosomes during the elongation cycle, and termed subunit rolling (12). The remaining 6% of particles aligned poorly and potentially represent a continuum of less well-populated states.

In bacterial ribosomes alongside the ratchet-like subunit rearrangement, the head domain can swivel by a further 6-7° (13). We observe only slight rotational movement of the head domain of the mt-SSU rRNA (1-2°), which may result from additional proteins elements connecting the head and body, particularly mS37 and uS5m. mS29, which forms mitochondria-specific bridges with the central protuberance of the mt-LSU is displaced by up to 3.4 Å between the three classes, in a movement independent of the rRNA head orientation (Fig. S9B).

Intersubunit bridges

The two ribosomal subunits are connected by a number of intersubunit bridges, although their composition was unclear at lower resolution (14, 15). The movement of the two subunits relative to one another, and rearrangement of the bridges, is an intrinsic part of the mechanism of the ribosome. In bacteria and eukaryotes, these bridges consist mainly of conserved RNA-RNA interactions (16). In contrast, the interface of the mitoribosome has a far greater ratio of protein-mediated contacts, with three protein-protein and six protein-RNA bridges. The effect of the extensively remodeled bridges is an mt-SSU that can sample more conformational space than the bacterial ribosome.

Intersubunit bridges B1, B1b/c, B4, B6 and B8 that are found in bacterial and cytoplasmic ribosomes are absent from human mitoribosomes (Figs. 4 and S10). Based on class 1, which forms the largest interface between subunits, we define seven additional mitochondria-specific bridges (designated with the prefix m, Figs. 4, S11 and Table S4). The bridges occur along the long axis of the mt-SSU from the head to the lower body, although they are primarily centered on the central region of the body. Bridges mB1a and mB1b at the head of the mt-SSU are analogous to bacterial bridges B1a and B1b as they mediate interactions with the central protuberance of the LSU through mitochondria-specific proteins. At the lower body mB6 is formed between the N-terminal extension of bL19m and mS27.

Of the mitochondria-specific bridges, mB4 buries the largest surface area and is formed by an interaction between mS38 and mt-LSU rRNA H71. At the interface, a helical element of mS38 runs parallel to the upper part of h44 before a 90° kink with the N-terminus protruding into the mt-SSU rRNA (Fig. 5A-B). Its location and structure resembles eL41, a short basic α-helix that forms a eukaryotic-specific bridge (eB14) in the cytoplasmic ribosome (17) suggesting that mS38 and eL41 are the products of convergent evolution. Although the length of eL41 and the contacts it makes with the two subunits vary among species (18), mS38 is substantially longer and the helix that runs parallel to the interface is specific to mitoribosomes as it fills a space generated by the absence of mt-LSU rRNA H62.

With the exception of the pivot, bridge B3 that maintains nearly identical contacts in all observed classes, the other bridges form dynamic communication pathways (Table S5). The bridges at the head and bottom of the mt-SSU are particularly dynamic, and are therefore poorly resolved. In the ratcheted state, a new bridge (mB7) is formed between uL2m and the phosphate backbone of h23. The rolling movement preserves the upper part of h44 and therefore its bridges with the mt-LSU.

A GTPase mediates intersubunit bridges with the central protuberance

In all domains of life, GTPase factors act on the ribosome at every stage of translation. However, mitoribosomes are the only ribosomes that have acquired an intrinsic GTPase activity through the GTP-binding protein, mS29 (19). In mice, mS29 deficiency is lethal *in utero* with abnormal, shrunken mitochondria (20). We located mS29 to the mt-SSU head close to the subunit interface (Fig. 5D-E) with density for a bound nucleoside diphosphate (Fig. S12). It is involved in coordinating two mitochondria-specific bridges (mB1a and mB1b) with elements of the remodeled central protuberance (Fig. S11, Table S4). Structurally, mS29 is similar to P loop-containing nucleoside triphosphate hydrolases and possesses both Walker A and B motifs (residues 128-135 and 249-263, respectively) that are necessary for catalysis (21), suggesting that mS29 is catalytically active. The structure also reveals that a hydrogen bond between the carbonyl group of GTP and the main chain amide of Met100 (Fig. S12B) is responsible for the specificity of the mitoribosome for guanosine over adenosine (19).

The presence of GDP bound to mS29 at the subunit interface suggests that GTPase activity is linked to subunit association, which is compatible with the observation that although the

mt-SSU readily binds GTP, the intact mitoribosome does not (19) as the γ-phosphate would clash with Thr313.

The mRNA channel

During translation the mRNA occupies an RNA-rich groove that encircles the neck of the SSU (22). The human mitoribosome has substantial differences in both the entry and exit sites of this channel compared to other ribosomes (Fig. 6). In bacterial ribosomes, incoming mRNA passes through a ring-shaped entrance formed by uS3, uS4 and uS5 that is located between the head and shoulder of the SSU. Basic residues from uS3 and uS4 confer helicase-like activity on the ribosome that unwinds secondary structure present in the mRNA (23). In the human mitoribosome, the entry site has been remodeled due to the absence of uS4 and deletion of the C-terminal domain of uS3. The new entry site is dominated by an extension to uS5m that partially compensates for the lack of uS4 and interacts with uS3m (Fig. 6A). As a result, the entrance has shifted and its diameter expanded from 9 to 15 Å (Fig. S13A-B). The interior of the channel is lined with basic (Arg189, Lys239, Arg264) and aromatic (Phe229) residues from uS5m, which might be involved in direct interactions with mRNA (Fig. S13C).

While the entrance has widened, the average diameter of the channel is still less than that of an RNA duplex. Therefore mRNAs must enter as a single strand. In the proximity of the channel entrance is a pentatricopeptide repeat (PPR) protein (mS39) bound to the solvent side of the head (Fig. 6B). This is the largest protein of the mt-SSU and comprises a helix-turn-helix array stretching over 110 Å. Its knockdown results in a significant overall decrease in mitochondrial protein synthesis (24). A conserved property of PPR proteins is the ability to bind single-stranded RNA (25) including the 5′ ends of mRNA (26). In our structure, the RNA-binding motifs closest to the channel entrance are solvent-exposed and remain unoccupied.

The exit from the channel between the head and platform is important for bacterial translation initiation. In bacteria, the Shine-Dalgarno sequence base pairs with the otherwise flexible 3′ end of SSU rRNA to specify the position of the start codon (22). Human mt-mRNAs lack a Shine-Delgarno sequence and are mostly leaderless (27), therefore the 3′ end of rRNA is not expected to be involved in initiation. Indeed, in the mitoribosome, this region is deleted and the 3′ end of rRNA is stably associated with mS37. This represents an example of convergent evolution with the eukaryotic ribosome, which also does not require a Shine-Dalgarno for initiation, where the function of locking the 3′ end of rRNA performed by eS26 (28).

At the channel exit, there is a protein with a single oligonucleotide-binding (OB) fold that is consistent with a low-resolution EM reconstruction (EMD-5693) and biochemical data (29) for a homolog of the N-terminal domain of bS1 (Fig. S14). Unlike bacterial bS1, bS1m is tightly associated with the ribosome through extensive interactions with uS2m and bS21m (Fig. 6B). In bacteria, bS1 is composed of six OB folds that work in a concerted manner to unfold mRNAs for active translation (30). We can exclude the possibility that bS1m forms a platform for bS1-like assembly, as it lacks the essential solvent exposed helix that forms the

interaction with the following OB domain (31) (Fig. S14D). However, the structural and positional conservation of bS1m with bS1 and a large electropositive patch that faces the emerging mRNA suggests a role in binding RNA (Fig. S14E-F).

Antibiotic sensitivity and effect of ribosomal mutations

Aminoglycosides are potent antibiotics for combating severe bacterial infections (32), and are also used for treatment of genetic disorders (33). Mutations in the mt-SSU rRNA gene, particularly A1555G and C1494T, have been reported to predispose carriers to aminoglycoside hypersensitivity linked to increased ototoxicity and nephrotoxicity (34). The structure reveals that these two mutations would re-introduce base pairs to limit the increased flexibility of the decoding center and resemble more closely the aminoglycoside-binding site in bacterial ribosomes (35) (Fig. S15A). Since the clinical use of aminoglycosides and oxazolidinones (Fig. S15B) are limited by toxicity due to inhibition of mitoribosomes (34, 36), the structure will aid the rational design of more selective compounds. Similarly, the structure provides a reference for the analysis of mitoribosomal mutations that cause severe pathologies (Table S6 and Fig. S16).

Supplementary Material

Refer to Web version on PubMed Central for supplementary material.

Acknowledgements

References

1. Amunts A, et al. Science. 2014; 343:1485. [PubMed: 24675956]

2. Brown A, et al. Science. 2014; 346:718. [PubMed: 25278503]

3. Greber BJ, et al. Nature. 2014; 515:283. [PubMed: 25271403]

4. Zhang W, Dunkle JA, Cate JH. Science. 2009; 325:1014. [PubMed: 19696352]

5. Heublein M, et al. Mol Biol Cell. 2014; 25:3342. [PubMed: 25165143]

6. SOM,

7. Chen Y, Feng S, Kumar V, Ero R, Gao YG. Nat Struct Mol Biol. 2013; 20:1077. [PubMed: 23912278]

8. VanLoock MS, et al. J Mol Biol. 2000; 304:507. [PubMed: 11099376]

9. Selmer M. Science. 2006; 313:1935. [PubMed: 16959973]

10. Tourigny DS, Fernandez IS, Kelley AC, Ramakrishnan V. Science. 2013; 340:1235490. [PubMed: 23812720]

11. Dunkle JA, Wang L, Feldman MB, Pulk A, Chen VB. Science. 2011; 332:981. [PubMed: 21596992]

12. Budkevich TV, et al. Cell. 2014; 158:121. [PubMed: 24995983]

13. Mohan S, Donohue JP, Noller HF. Proc Natl Acad Sci USA. 2014; 111:13325. [PubMed: 25187561]

14. Sharma MR, et al. Cell. 2003; 115:97. [PubMed: 14532006]

15. Kaushal PS, et al. Proc Natl Acad Sci USA. 2014; 111:7284. [PubMed: 24799711]

16. Chen J, Tsai A, O'Leary SE, Petrov A, Puglisi JD. Curr Opin Struct Biol. 2012; 22:804. [PubMed: 23142574]

17. Ben-Shem A, et al. Science. 2011; 334:1524. [PubMed: 22096102]

18. Wong W, et al. Elife. 2014:e03080. [PubMed: 24913268]

19. Denslow ND, Anders JC, O'Brien TW. J Biol Chem. 1991; 266:9586. [PubMed: 2033053]

20. Kim HR, et al. FASEB J. 2007; 21:188. [PubMed: 17135360]

21. Walker JE, Saraste M, Runswick MJ, Gay NJ. EMBO J. 1982; 1:945. [PubMed: 6329717]

22. Yusupova GZ, Yusupov MM, Cate JH, Noller HF. Cell. 2001; 106:233. [PubMed: 11511350]

23. Takyar S, Hickerson RP, Noller HF. Cell. 2005; 120:49. [PubMed: 15652481]

24. Davies SM, et al. FEBS Lett. 2009; 583:1853. [PubMed: 19427859]

25. Yin P, et al. Nature. 2013; 504:168. [PubMed: 24162847]

26. Manavski N, Guyon V, Meurer J, Wienand U, Brettschneider R. Plant Cell. 2012; 24:3087. [PubMed: 22773745]

27. Montoya J, Ojala D, Attardi G. Nature. 1981; 290:465. [PubMed: 7219535]

28. Rabl J, Leibundgut M, Ataide SF, Haag A, Ban N. Science. 2011; 331:730. [PubMed: 21205638]

29. Byrgazov K, Manoharadas S, Kaberdina AC, Vesper O, Moll I. PLoS ONE. 2012; 7:e32702. [PubMed: 22412910]

30. Qu X, Lancaster L, Noller HF, Bustamante C, Tinoco IJ. Proc Natl Acad Sci U S A. 2012; 109:14458. [PubMed: 22908248]

31. Takeshita D, Yamashita S, Tomita K. Nucleic Acids Res. 2014; 42:10809. [PubMed: 25122749]

32. Caminero JA, Sotgiu G, Zumla A, Migliori GB. Lancet Infect Dis. 2010; 10:621. [PubMed: 20797644]

33. Keeling KM, Wang D, Conard SE, Bedwell DM. Crit Rev Biochem Mol Biol. 2012; 47:444. [PubMed: 22672057]

34. Selimoglu E. Curr Pharm Des. 2007; 13:119. [PubMed: 17266591]

35. Qian Y, Guan MX. Antimicrob Agents Chemother. 2009; 53:4612. [PubMed: 19687236]

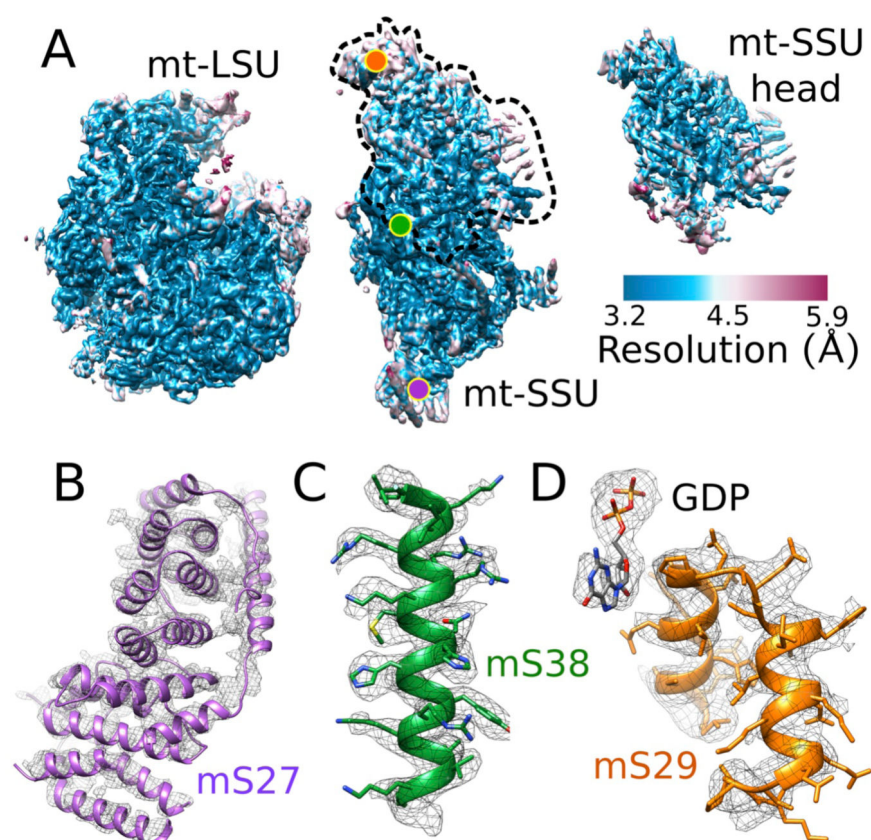36. Soriano A, Miro O, Mensa J. N Engl J Med. 2005; 353:2305. [PubMed: 16306535]

Fig. 1. Map quality

A. Maps generated using masked refinement colored by local resolution. The outline of the mask applied to the head is shown as a dashed line. Colored circles pinpoint the location on the mt-SSU of the density examples shown in panels B-D. **B**. Density for mS27 at the bottom of the mt-SSU. **C**. Well-resolved density for mS38 in the core of the mt-SSU. **D**. Density for mS29 including the bound GDP at the head.
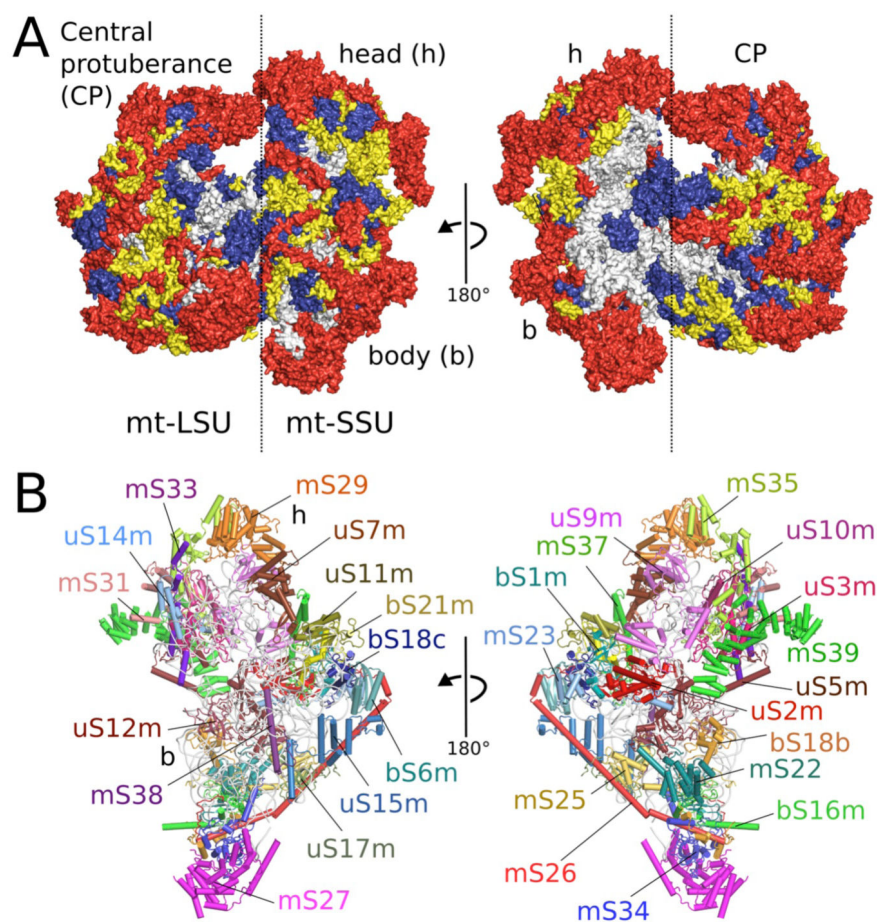
Fig. 2. Overview of the human mitoribosome

A. Proteins conserved with bacteria (blue), extensions of homologous proteins (yellow) and mitochondria-specific proteins (red). rRNA is shown in gray. **B**. Location of proteins in the human mt-SSU.
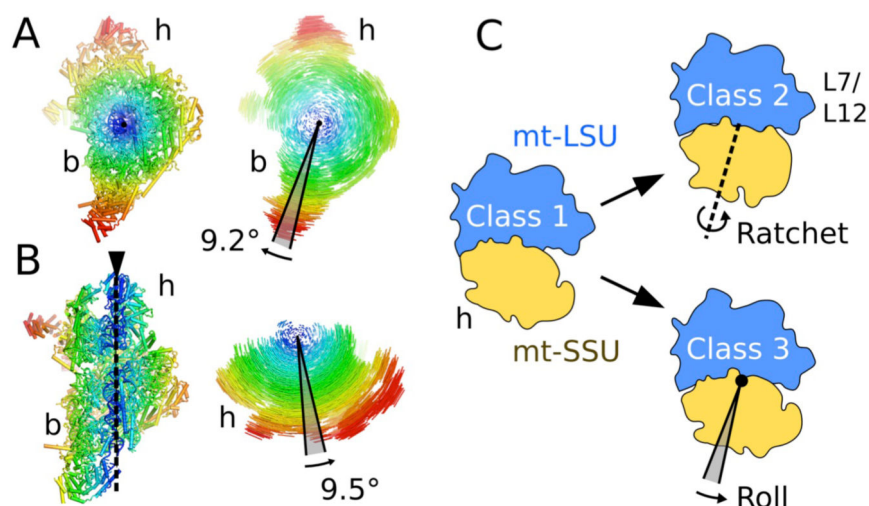
Fig. 3. Dynamics of intersubunit orientations
A-B. Comparison of mt-SSU orientations based on common superposition of the mt-LSU. Shifts between equivalent rRNA phosphorus atoms and protein Cα atoms in the different states are color-coded (0-20 Å). **A.** Intersubunit rotation resembling the ratchet-like mechanism common to all ribosomes. **B**. Rotation of the small subunit around its long axis. **C**. Schematic of mitoribosomal conformational changes.
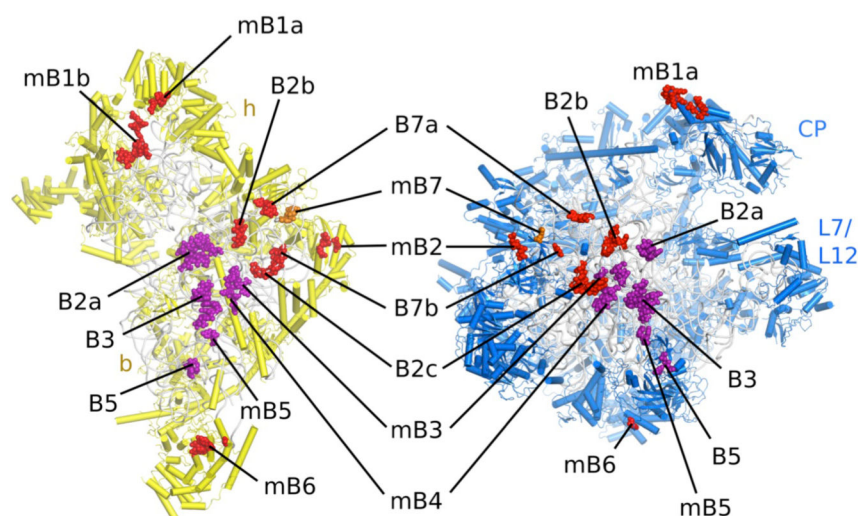
Fig. 4. Distribution of intersubunit bridges
View showing subunit interfaces; residues that form bridges are shown as spheres. Bridges invariant in all classes are shown in purple and dynamic bridges in red. mB7 is specific to class 2 and shown in teal.
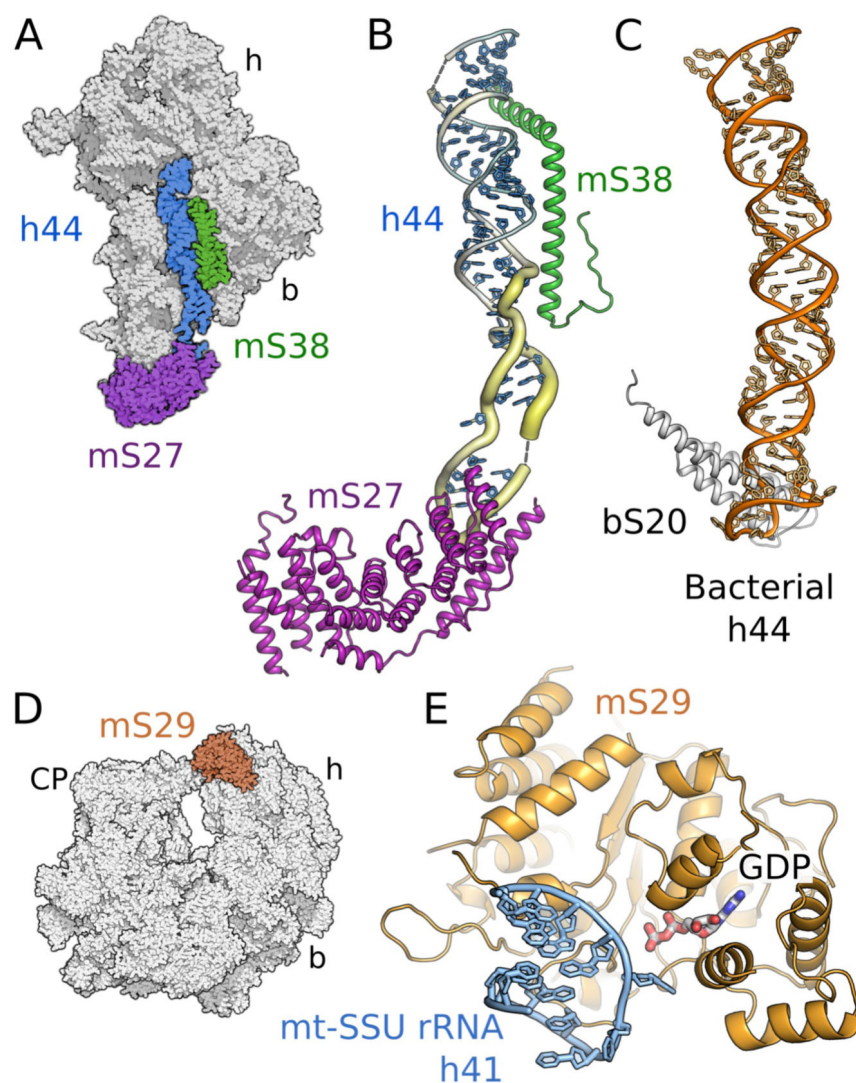
Fig. 5. Mitochondria-specific features at the subunit interface
A. h44, mS38 and mS27 coordinate novel bridges with the mt-LSU. **B**. h44 has been extensively remodeled. The upper half is stabilized by mS38, while the lower half has greater flexibility (the representation of the phosphate backbone is colored and sized by B factor). **C**. h44 in bacterial ribosomes. **D**. mS29 mediates mitochondria-specific bridges between the central protuberance and head. **E**. In monosomes, mS29 is bound to GDP.
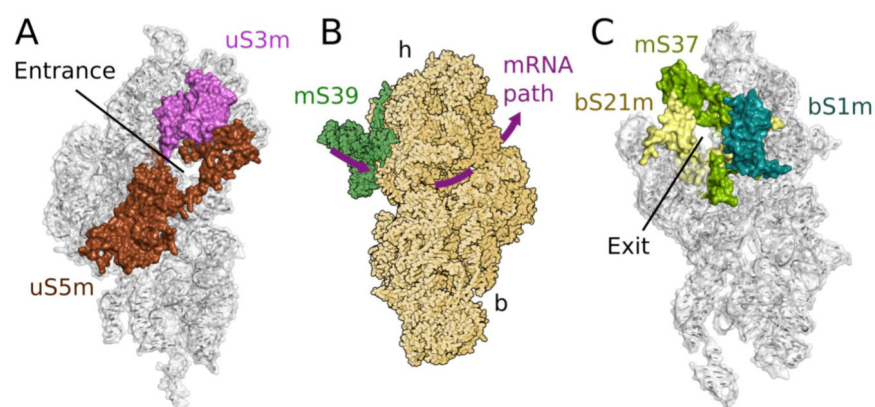
Fig. 6. Remodeling of the mRNA channel
A. A wide entrance to the mRNA channel is formed by uS3m and uS5m. **B**. Overall path taken by mRNA in the human mitoribosome with mS39 located near the channel entrance. **C**. mRNA emerges through an exit formed by bS1m, bS21m, and mS37.